ChemPubSoc Europe

DOI: 10.1002/ejic.201600591

EurJIC European Journal of Inorganic Chemistry

Full Paper

Siloxanes

3,5-Dimethylpyrazolyl-Substituted Di- and Trisiloxanes

Florian Bitto,*[a] Erica Brendler,[b] Uwe Böhme,[a] Jörg Wagler,[a] and Edwin Kroke*[a]

Abstract: The synthesis and characterization of di- and trisiloxanes with 3,5-dimethylpyrazolyl (pz*) moieties are presented. Disiloxanes of the type $O(SiMe_{3-n}pz^*_n)_2$ (n = 1, 2, and 3 in **2**, **3**, and **4**, respectively) are easily accessible through a *trans*-silylation approach. Crystal structure analyses of compound **4** and the two side products **5** and **6** illustrate different coordination motifs of pz* (terminal vs. bridging) in the disiloxane system. The reaction of $O_2Si_3Cl_8$ with Me_3Sipz^* led to the unsymmetrically substituted trisiloxane $pz^*_3SiO\text{-}Sipz^*_2O\text{-}SiCl_2pz^*$ (**7**) with bridging pz* units and tetra- and pentacoordinate silicon atoms and the fully pyrazolyl-substituted trisiloxane $O_2Si_3pz^*_8$ (**8**), depending on the choice of the reaction conditions. The ^{29}Si NMR properties of **7** were investigated by ^{29}Si CP/MAS NMR spectroscopy and supporting quantum chemical calculations analyzing the principal components of the chemical-shift tensor for all three silicon atoms in this molecule.

Introduction

Pyrazole and pyrazolide compounds show manifold coordination modes in complexes with transition metals.[1a] As parts of boron-, carbon-, and silicon-based compounds, pyrazolyl units also show interesting ligand characteristics due to their multiple coordination possibilities.[1b–1f] In our previous studies on the chemistry of pyrazolyl-substituted silicon compounds, we investigated the reactivity of hydridochlorosilanes and disilanes.[2] We identified siloxanes with pyrazolyl units as potential new multidentate ligands for transition metals. Therefore we expanded our investigations to the reactions of chloro-substituted disiloxanes $O(SiMe_{3-n}Cl_n)_2$ (n = 1, 2, 3) and octachlorotrisiloxane $O_2Si_3Cl_8$ with Me_3Sipz^*. None of the potential products are known in the literature. Only a scarce set of examples of disiloxanes and trisiloxanes substituted by Si–N-bound five-membered heterocycles has been published so far, that is, siloxanes functionalized with pyrrolidinonyl (**I** to **III**)[3] phthalimidyl (**IV**),[4] pyrrolyl (**V**),[5] and imidazolyl groups (**VI**)[6] (Scheme 1).

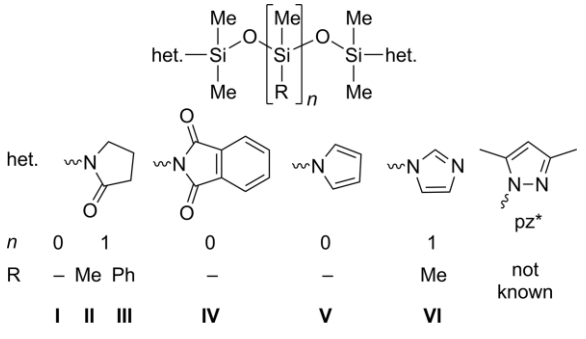

Scheme 1. Di- and trisiloxanes substituted by five-membered heterocycles.

Results and Discussion

Substituted Disiloxanes

The pz*-substituted disiloxanes were prepared from the corresponding chloro-substituted siloxanes. In the disiloxane series $O(SiMe_{3-n}Cl_n)_2$ (n = 1, 2, 3) the compounds with n = 1 and 3 were commercially available. 1,1′,3,3′-Tetrachloro-1,3-dimethyldisiloxane $O(SiMeCl_2)_2$ (**1**) had to be synthesized for our studies. Even though the literature provides a selection of routes to **1** (from the high-boiling fraction of the Müller–Rochow process,[7] chlorination of hydrogen-substituted siloxanes,[8] and partial hydrolysis of methyltrichlorosilane[9]), these methods have low selectivity, low yield, and/or laborious purification in common. Therefore, we employed the Friedel–Crafts acylation method for replacing *Si*-bound phenyl substituents by Si–Cl bonds (Scheme 2).[10] To the best of our knowledge this is the first report on a siloxane being chlorinated in this manner. Notably, in *n*-hexane as solvent this reaction of 1,1,3,3-tetraphenyl-1,3-dimethyldisiloxane $O(SiMePh_2)_2$ and stoichiometric amounts of $AlCl_3$ (anhydrous) and acetyl chloride proceeds in a clean manner and was completed within minutes.

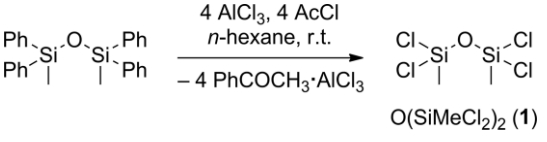

Scheme 2. Synthesis of **1** by Friedel–Crafts acylation.

The isolation of the pure disiloxane **1** from this reaction mixture is laborious due to carryover by *n*-hexane (see Experimental Section and Supporting Information for details). However, as

[a] *Institut für Anorganische Chemie, TU Bergakademie Freiberg, Leipziger Str. 29, 09599 Freiberg Germany*
E-mail: florian.bitto@chemie.tu-freiberg.de
edwin.kroke@chemie.tu-freiberg.de
www.tu-freiberg.de/fakult2/aoch/agsi
[b] *Institut für Analytische Chemie, TU Bergakademie Freiberg, Leipziger Str. 29, 09599 Freiberg Germany*
Supporting information and ORCID(s) from the author(s) for this article are available on the WWW under http://dx.doi.org/10.1002/ejic.201600591.

the raw product is a two-component mixture of *n*-hexane and **1** (according to NMR spectroscopic analysis), we decided to use this hexane solution of **1** (after gas chromatographic analysis) in subsequent stoichiometric reactions.

The disiloxanes of the type $O(SiMe_{3-n}pz^*_n)_2$ **2** (n = 1), **3** (n = 2), and **4** (n = 3) were synthesized by a *trans*-silylation approach with Me_3Sipz^* in *n*-hexane (Scheme 3). The compounds were isolated by removal of the solvent and the volatile byproduct Me_3SiCl in vacuo. Compounds **3** and **4** are colorless solids, and **2** was obtained as a colorless liquid. The identity of the compounds was confirmed by multinuclear NMR spectroscopy ($^{29}Si\{^1H\}$, $^{13}C\{^1H\}$, ^1H), Raman spectroscopy, and elemental analyses.

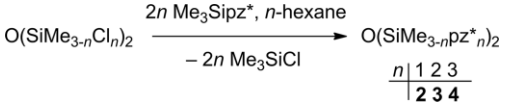

Scheme 3. Synthesis of the disiloxanes **2**, **3**, and **4**.

^{29}Si NMR spectroscopy revealed an upfield shift of the resonance on replacing Si–Cl by Si–pz* for each set of disiloxanes (Table 1).

Table 1. ^{29}Si NMR shifts [ppm] of the series of disiloxanes $O(SiMe_{3-n}R_n)_2$ (n = 1–3, R = pz*, Cl) recorded in C_6D_6.

	$O(SiMe_2R)_2$	$O(SiMeR_2)_2$	$O(SiR_3)_2$
R = Cl	6.6	–15.0	–45.3
R = pz*	–6.1	–36.2	–77.6

Compound **4** was also characterized by single-crystal XRD. Suitable crystals were obtained by recrystallization from *n*-hexane. The structure was refined in the triclinic space group $P\bar{1}$ with one half-molecule in the asymmetric unit (Figure 1).

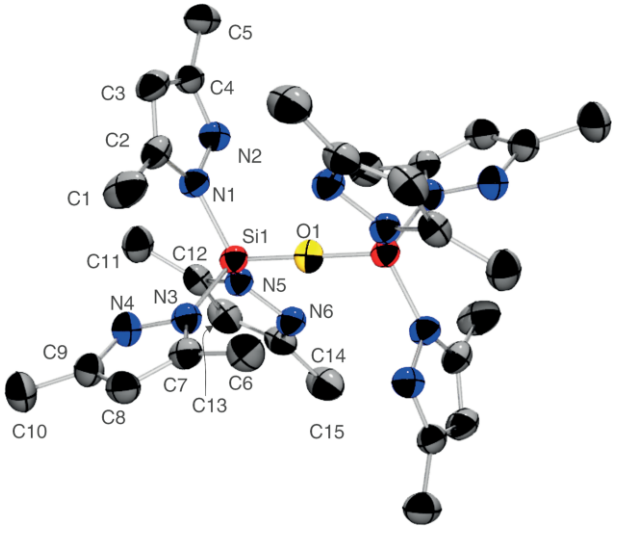

Figure 1. Molecular structure of **4** in the crystal (ellipsoids set at 50 %, hydrogen atoms omitted for clarity).

The Si–O–Si angle is constrained to 180° due to positioning of the oxygen atom on a crystallographic center of inversion. The larger thermal displacement factor of O1 [U_{iso} = 41(1)] with respect to that of Si1 [35(1)], however, hints at dynamic disorder of the oxygen position, and thus a significant deviation of the Si–O–Si angle from linearity. Wojnowski et al. have demonstrated the influence of this centrosymmetric constraint of a disiloxane O atom in $O[Si(OtBu)_3]_2$.[11] Initial refinement in the space group $P\bar{1}$ gave an Si–O–Si angle of 180°, but with large and very anisotropic thermal ellipsoid for the oxygen atom [U_{11} = 143(6), U_{22} = 212(8), U_{33} = 57(4), U_{eq} = 138(4)] indicating enhanced mobility. They are also much larger than that of the silicon atoms [U_{eq}(Si) = 71(1)].

Much better results were obtained by refinement of a disorder model (rigid-body model), which decreased the Si–O–Si angle to 144°. Unfortunately, neither structure refinement in a lower-symmetry space group ($P1$) nor refinement of split positions for O1 proved suitable to solve this problem.

Therefore, we employed quantum chemical methods to address this issue and to obtain information regarding the true Si–O–Si angle. The variation of the Si–O–Si angle in **4** was calculated by means of a relaxed potential-energy surface (PES) scan at the B3PW91-6-31G(d) level of theory (for details, see Supporting Information). Bending of the Si–O–Si angle revealed a very flat PES between 170 and 180° with the minimum at 175° (Figure S9 and Table S2). This explains the rather large anisotropic thermal ellipsoid for the oxygen atom in the X-ray structure of **4**. These results are in line with findings from quantum chemical calculations on a range of disiloxanes $O(SiR_3)_2$ (R = H,[12,13] F,[13] Cl,[13] Me,[13] OH[14]) at the DFT and MP2 levels of theory. The results consistently show a flat PES in the range of 140–180° with a barrier of 5–10 kJ/mol for linearization. This low barrier enables great mobility of this unit. Hence, the crystallographically imposed Si–O–Si angle of 180° in **4** does not reflect the true situation, but calculations confirmed the true angle (energetic minimum) to be close to 180°. The negative hyperconjugation from the oxygen lone pairs to the $Sipz^*_3$ units stabilizes this almost linear arrangement.

The coordination geometry around the silicon atom is best described as a distorted $Si(N_3O)$ tetrahedron with N–Si–N(O) angles in the range of 106.91(6)–111.21(6)°. The pyrazolyl ring at N1 is nearly perpendicular to the Si–O bond [O1–Si1–N1–N2 74.64(13)°], while the other two rings show *cis* (N3–N4) and *trans* orientation (N5–N6) of their second N atom with respect to the Si–O bond [O1–Si1–N5–N6 30.84(12)°, O1–Si1–N3–N4 –168.56(10)°]. The two $Sipz^*_3$ moieties adopt a pseudostaggered conformation along the central Si–O–Si unit. The Si–N bond lengths [1.728(1) Å–1.737(2) Å] are in line with those of other silicon compounds with terminal pz* units.[2,15] The Si–O bond length [1.593(1) Å] is slightly shorter than that of $O(SiPh_3)_2$ [1.616(1) Å], which conforms to the higher electronegativity of the substituents in **4**.[16]

Our attempts at synthesizing partially pz* substituted disiloxanes by treating $O(SiCl_3)_2$ with substoichiometric amounts of Me_3Sipz^* failed (we did not succeed in isolating defined compounds). These reactions produced mixtures of partially substituted chlorosiloxanes and compound **4**. Nonetheless, our attempts to isolate pure compounds by recrystallization resulted in small amounts of crystals of decomposition products $[(\mathbf{4})(\mathbf{5})_2$ and **6**]. Their molecular structures demonstrate the variable coordination modes of *Si*-bound pz* units. They complement the

terminal bonding mode in **4** by a bridging mode of pz* and, as their characteristic feature as hydrolysis products, ligation by Hpz*. [(μ-pz*)$_2$(O){SiCl$_2$(Hpz*)}$_2$] (**5**) is an Hpz* adduct of the intended partially pz* substituted siloxane O(SiCl$_2$pz*)$_2$ and co-crystallizes with **4** as (**4**)(**5**)$_2$ in the monoclinic space group *C*2/*c*. The asymmetric unit consists of one half-molecule of **4** and one molecule of **5**. The two silicon atoms in **5** are octahedrally coordinated by their mutual O atom, two chloro substituents, two bridging pyrazolyl units, and a coordinated Hpz* molecule (Figure 2).

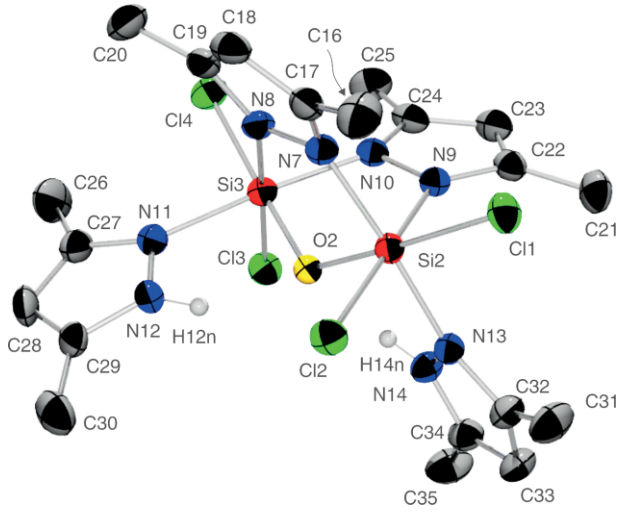

Figure 2. Molecular structure of **5** in a crystal of (**4**)(**5**)$_2$ (ellipsoids set at 50 %, *C*-bound hydrogen atoms omitted for clarity). The *N*-bound hydrogen atoms were located as residual electron-density peaks.

Compared with the other disiloxanes discussed here, the Si–O–Si angle in **5** is noticeably small [120.35(14)°] because of its location in a five-membered ring system, and the Si–O bonds are the longest because of the hexacoordination of the Si atoms. The molecular structure of **5** is stabilized by intramolecular N–H···Cl hydrogen bonds [H12n···Cl2 2.55 Å, N12–H12n···Cl2 170.1°, H14n···Cl3 2.68 Å, N14–H14n···Cl3 174.4°].

The second side product **6** is also an Hpz* adduct of disiloxane O(SiCl$_2$pz*)$_2$, but features only one Hpz* ligand and only one bridging pz* group, whereas the second pz* substituent is terminal. It crystallized directly from the reaction solution in *n*-hexane in monoclinic space group $P2_1/m$ (Figure 3). The asymmetric unit contains one half-molecule, which is located on a bisecting plane with most of its atoms; only the Cl atoms are out of this plane. The coordination around the silicon atoms is nearly ideal trigonal-bipyramidal [τ(Si1) = 0.98, τ(Si2) = 0.97][17] with N–Si–N axes. The structure features a N–H···N hydrogen bond between the terminal pz* unit and the coordinated Hpz* moiety [N4–H4n···N6 171.71°, H4n···N6 2.01 Å] which stabilizes this flat conformation.

Table 2 compares structural data for **4**–**6**.

Compounds **4**–**6** reflect different coordination modes of the pyrazolyl unit: pz* as terminal substituent or in a bridging mode between two silicon atoms, and Hpz* as a bifunctional ligand having a polar N–H bond available for establishing N–H···Cl/N hydrogen bonds, which enhances the binding of this ligand in addition to its primary N–Si coordination.

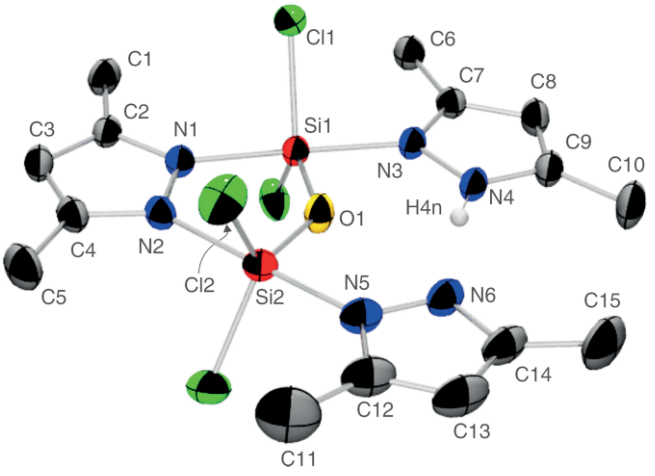

Figure 3. Molecular structure of **6** (ellipsoids set at 50 %, *C*-bound hydrogen atoms omitted for clarity).

Table 2. Comparison of structural features of compounds **4**, **5**, and **6**.

	4		**5**		**6**	
Si–N [Å]	N1	1.734(2)	N7	1.915(3)	N1	1.881(1)
	N3	1.737(2)	N8	1.921(3)	N2	1.927(2)
	N5	1.728(2)	N9	1.923(3)	N3	1.913(2)
			N10	1.927(3)	N5	1.853(2)
			N11	1.946(3)		
			N13	1.948(3)		
Si–O [Å]		1.594(1)	Si2	1.673(3)	Si1	1.624(1)
			Si3	1.680(2)	Si2	1.636(1)
Si–O–Si [°]		180		120.35(14)		133.51(9)

Substituted Trisiloxanes

Our initial aim was to synthesize the fully pz*-substituted trisiloxane O$_2$Si$_3$pz*$_8$ (**8**). During the experiments we found that the solvent (solv) is the most important factor for success. Using *n*-hexane, *n*-pentane, or diethyl ether did not lead to the desired product **8** but yielded the asymmetrically substituted trisiloxane **7** (Scheme 4).

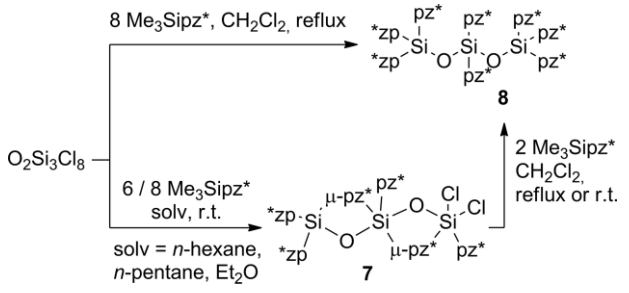

Scheme 4. Synthesis of **7** and **8** by a one- or two-stage *trans*-silylation process.

The fully pz* substituted siloxane can be prepared by *trans*-silylation in dichloromethane. Product **7**, obtained by *trans*-silylation in the above-mentioned solvents, can be converted to **8** in a second stage *trans*-silylation reaction. Both trisiloxanes were characterized by multinuclear NMR spectroscopy (^{29}Si{^{1}H}, ^{13}C{^{1}H}, ^{1}H), Raman spectroscopy, and elemental analysis. For **7**

the single-crystal structure and ^{29}Si CP/MAS NMR spectrum of the crystalline compound were obtained.

Compound **7** crystallizes in the triclinic space group $P\bar{1}$ with one molecule in the asymmetric unit directly from the reaction mixture in *n*-hexane (Figure 4).

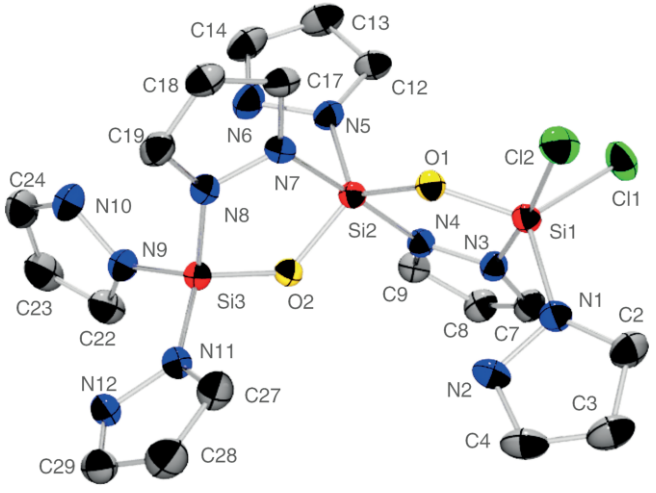

Figure 4. Molecular structure of **7** (ellipsoids set at 50 %, hydrogen atoms and methyl groups of the pz* units are omitted for clarity).

Silicon atoms Si1 and Si2 adopt distorted trigonal-bipyramidal coordination spheres [τ(Si1) = 0.88, τ(Si2) = 0.92] with Cl2–Si1–N3 and N4–Si2–N7 as the axes. The coordination environment around the third silicon atom is best described as pseudotetrahedral [N–Si3–N(O) 97.46°···115.06°]. The Si–N bonds of the nitrogen atoms that occupy the axial positions of the trigonal bipyramids (N3, N4, N7) are significantly longer than the other Si–N bonds in the molecule (Table 3). This is in accord with structural data from the literature and the concept of 3c–4e bonds in the axial position of trigonal-bipyramidal silicon complexes.[18] The Si–O bond lengths and Si–O–Si angles (Table 3) are in line with those found for compounds **5** and **6**.

Table 3. Selected bond lengths [Å] and angles [°] in the structure of **7**.

	Atoms		Value
Si–N	Si1	N1	1.769(1)
		N3	1.933(1)
	Si2	N4	1.870(1)
		N5	1.770(1)
		N7	1.950(1)
	Si3	N8	1.749(1)
		N9	1.721(1)
		N11	1.729(1)
Si–O	Si1	O1	1.645 (1)
	Si2	O1	1.639 (1)
		O2	1.669 (1)
	Si3	O2	1.618 (1)
Si–O–Si		O1	133.58(6)
		O2	125.20(6)

To assign the ^{29}Si NMR signals to the individual Si atoms of **7**, two of which are pentacoordinate, we combined ^{29}Si CP/MAS NMR spectroscopy for determination of the principal components of the chemical-shift anisotropy (CSA) tensor with the results of quantum chemical calculations. The CP/MAS NMR spectra were recorded at different spinning frequencies (1.3, 2.3, 5 kHz). The three isotropic shifts (δ = –63.4, –123.8, and –135.2 ppm) are in accord with the expected three signals of one tetra- and two pentacoordinate silicon atoms. The signal broadening of the peak at δ = –123.8 ppm, which can be attributed to residual dipolar coupling to the quadrupolar chlorine nuclei, already hints at an assignment of this signal to the chloro-substituted Si atom Si1. This assignment was then confirmed by the agreement of the principal components of the CSA tensors of the three Si atoms extracted from the spinning-sideband spectra and the corresponding data predicted by computational methods (Table 4 and Figure S3).[19,20]

Table 4. Experimental and calculated ^{29}Si CSA tensor principal components δ_{11}, δ_{22}, δ_{33} and parameters derived therefrom (isotropic shift δ_{iso}, span Ω, skew κ) of compound **7**.[21]

Si		δ_{iso}	δ_{11}	δ_{22}	δ_{33}	Ω	κ
Si1	exp.[a]	–123.8	–16.7	–157.6	–195.6	178.8	–0.58
	calcd.[b]	–116.3	–4.7	–159.2	–185.2	180.5	–0.71
Si2	exp.	–135.2	–26.4	–173.4	–205.9	179.5	–0.64
	calcd.	–140.9	–25.6	–185.7	–211.3	185.7	–0.72
Si3	exp.	–63.4	–29.3	–64.4	–96.1	66.3	0.04
	calcd.	–66.9	–33.3	–63.8	–103.7	70.4	0.13

[a] Experimental: extracted from the ^{29}Si CP/MAS data at a spinning frequency of 2.0 kHz. [b] Calculated: B3PW91/6-311+G(2d,p) using the atomic coordinates from the crystal structure.

The signal at δ = –63.4 ppm is easily related to Si3 in the crystal structure, which is the only four-coordinate silicon atom. Taking into account the results of the quantum chemical calculations [B3PW91/6-311+G(2d,p), calculated with the coordinates of the crystal structure], the other two peaks can now be assigned to Si1 ($OSiCl_2pz^*$, –123.8 ppm) and Si2 ($O_2Sipz^*_2$, –135.2 ppm). ^{29}Si NMR spectroscopic data obtained for the disiloxanes already showed that pz*-substituted silicon atoms exhibit pronounced shielding with respect to similar chloro-substituted Si atoms. This is in agreement with the situation here: two silicon atoms in comparable bonding situation (five-coordinate, oxygen and chloro/pz* substituents), the one with more pz* units has an isotropic ^{29}Si NMR signal shifted to higher field.

Interestingly, the isotropic chemical shift is noticeably different for Si1 and Si2, whereas their contributors (principal components of the shift tensor) are simultaneously shifted, and thus the CSA tensors of Si1 and Si2 have very similar span and skew (in accord with the calculated data, Table 4). The influence of the different types of substituents with respect to the orientation of the CSA tensor components in the molecule (Figure 5) provides an explanation. For the pentacoordinate silicon atoms (Si1, Si2), the orientation of principal component δ_{11} corresponds to the axis of the trigonal bipyramid. The other two components are situated in the equatorial plane of the coordination environment. With the rather wide span and negative skew (one significantly less shielded direction, i.e., along the bipyramidal axis), the CSA tensors of Si1 and Si2 match the expected pattern for pentacoordinate silicon compounds.[22,23] It has been shown that the principal components of the shielding tensor are strongly influenced by the ligands that are perpendicular to them.[22,24] Thus, in case of Si1 and Si2, Si–Cl versus Si–N bonds have been exchanged both in equatorial and

axial position, and therefore greater shielding of Si2 in all directions is observed.

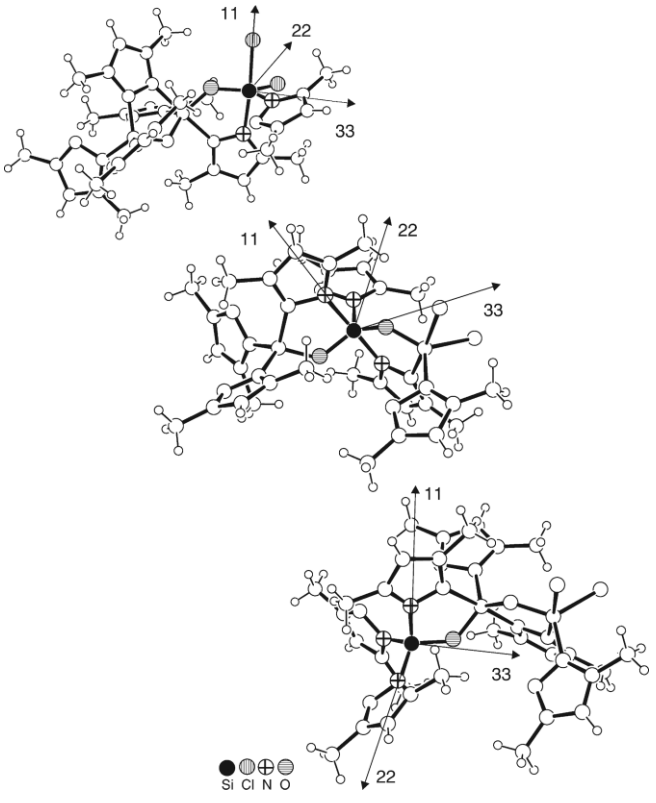

Figure 5. Orientation of the CSA tensor principal components (calculated) in **7** (Herzfeld–Berger convention);[19–21] from top to bottom: Si1, Si2, Si3. The arrows show only the direction not the magnitude.

Depending on the solvent, the ^{29}Si NMR spectrum of **7** in solution reveals complex dynamic behavior. This is not limited to the silyl transfer between the nitrogen atoms of the pz* units, as observed for pyrazolyl-substituted monosilanes,[25] it also includes changes in the coordination environment of the silicon atoms.

For solutions in C_6D_6 and THF, signals in the typical region of four- and five-coordinate silicon atoms are found (Table 5). The signal of the four-coordinate silicon atom is considerably shifted upfield compared to the solid state, while for the silicon atoms with higher coordination numbers two sets of signals can partially be observed (Figure 6). This is attributed to the presence of diastereomeric species, which originate from the change of the bridging pz* units between Si1 and Si2 or Si2 and Si3 by breaking the Si2–N4 and Si3–N8 bonds while forming Si2–N2 and Si3–N6 bonds. Unequal intensity of the signals is due to energetic differences between the isomers.

Table 5. ^{29}Si NMR shifts [ppm] of **7** in the solid state and in different solvents.

	Si1	Si2	Si3
CP/MAS	–123.8	–135.2	–63.4
C_6D_6	–120.9/–121.7	–133.2/–135.7	–68.9
THF	–122.5	–134.4/–137.2	–70.3

For a solution of **7** in $CDCl_3$ no ^{29}Si NMR signals could be observed. We attribute this to fast exchange between the different species, resulting in line broadening to an extent that prevents the detection of signals. This is supported by a comparison of the ^{1}H NMR spectra of **7** in C_6D_6 and $CDCl_3$ (Figure 7). The former shows narrow individual lines, indicating slow exchange, and the latter broad signals due to coalescence, typical for fast exchange.

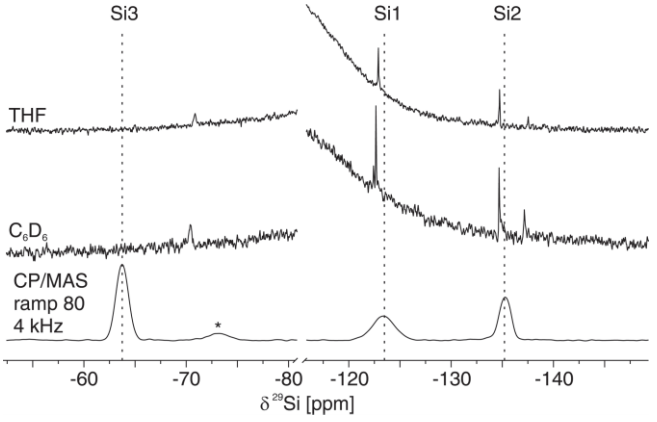

Figure 6. ^{29}Si NMR spectra of **7** in different solvents and in the solid state. For the purpose of comparison the positions of the signals of Si1, Si2, and Si3 (labels correspond to the crystal structure) are marked in the CP/MAS spectrum. The asterisk marks a spinning sideband of Si1.

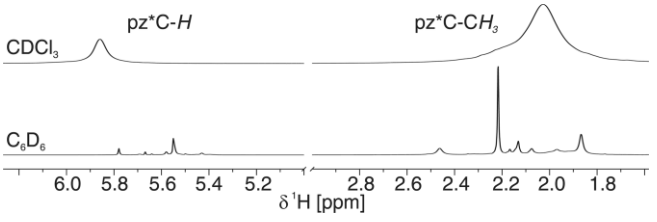

Figure 7. ^{1}H NMR spectra of **7** in the regions of the pz* signals.

The ^{29}Si NMR spectrum of the fully pz*-substituted trisiloxane **8** shows two signals in the upfield region of tetracoordinate Si atoms (Figure 8). The signals at δ = –77 and –91 ppm occur with an intensity ratio of 2:1 and are noticeably shifted upfield with respect to the starting material $O_2Si_3Cl_8$ (Cl_3SiO: –46.0 ppm, Cl_2SiO_2: –72.0 ppm, ratio 2:1). We assign the signal at δ = –77 ppm to the terminal silicon atoms (pz*$_3$SiO). The shift is similar to that of the pz*$_3$SiO group in the disiloxane **4** (δ = –77.6 ppm) and only slightly shifted upfield relative to that of **7**. The remaining upfield-shifted signal (δ = –91 ppm) is assigned to the central pz*$_2$SiO$_2$ unit. As for **7** no ^{29}Si NMR signal was obtained from a $CDCl_3$ solution of **8**. The solid-state NMR spectrum of **8** shows signals in the same region as that in benzene solution. The terminal –OSipz*$_3$ units show two signals of similar intensity. This could be due to inequivalence of the two terminal groups of one molecule in the solid state or different conformer sites (crystallographically independent molecules). The CP/MAS spectrum of **8** at 4 kHz shows no spinning sidebands and a small span comparable to that for Si3 in compound **7**. These are further hints at tetracoordination of all Si atoms.

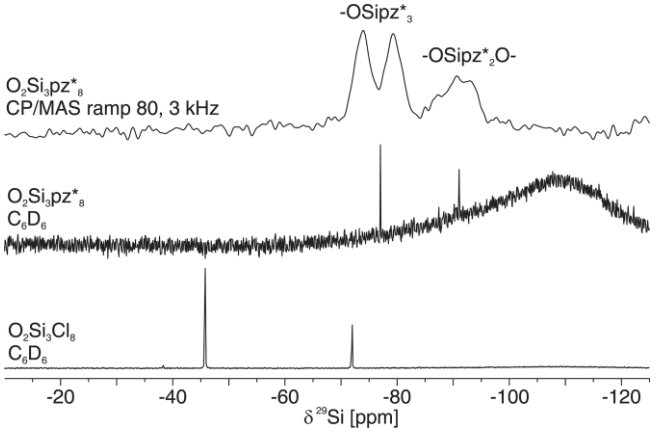

Figure 8. ^{29}Si NMR spectra of **8** and $O_2Si_3Cl_8$.

In spite of two out of three Si atoms having the same substitution pattern, the Si atoms of **7** exhibit different coordination features to those of **8**. For an explanation of the formation of the unusual compound **7** one must consider different aspects: 1) Me_3Sipz^* is a mild reagent, in contrast to pz*$^-$ (e.g., 3,5-dimethylpyrazole in the presence of triethylamine), as shown by the reaction with H_2SiCl_2 and $HSiCl_3$;[2] 2) the low solubility of **7** in some solvents helped with its isolation; 3) the formation of compound **8** is observed at room temperature only in CH_2Cl_2. This is in line with the results of calculations for the isodesmic reaction **7** → **8** (Scheme 5) at the B3PW91/6-31G(d) level of theory. The computational analysis predicts a positive small Gibbs free energy of +20 kJ/mol in the gas-phase and +28 kJ/mol in CH_2Cl_2, which disfavors the formation of **8** from **7**, but could still be compensated by solvent effects (for more details, see the Supporting Information).

$$\underset{\mathbf{7}}{O_2Si_3pz^*_6Cl_2} + 2\,Me_3Sipz^* \longrightarrow \underset{\mathbf{8}}{O_2Si_3pz^*_8} + 2\,Me_3SiCl$$

ΔG = + 20 kJ/mol (B3PW91/6-31G(d)), gas phase
+ 28 kJ/mol (B3PW91/6-31G(d)), CH_2Cl_2 (PCM model)

Scheme 5. Reaction leading from **7** to **8** for calculation of the Gibbs free energy.

Thus, both kinetic effects (poor solubility of **7** in some solvents, mild *trans*-silylation reagent pz*-$SiMe_3$) and thermodynamic effects (disfavored formation of **8**, unless compensated by favorable solvent effects) contribute to the formation and isolation of compound **7** and serve as an explanation why the choice of a different solvent eventually gave rise to the formation of **8**.

Conclusion

The synthesis of $O(SiMeCl_2)_2$ by Friedel–Crafts acylation is simple and effective. The procedure used by us results in the pure product or *n*-hexane solutions thereof. Both can be used for subsequent reactions. The pz*-substituted disiloxanes $O(SiMe_{3-n}pz^*_n)_2$ are easily obtained by *trans*-silylation with Me_3Sipz^*. Their ^{29}Si NMR signals are upfield-shifted with increasing replacement of Cl atoms by pz* units. The molecular structures determined for $O(Sipz^*_3)_2$ (**4**) and the two side products **5** and **6** demonstrate the coordinative possibilities of the (H)pz* unit in combination with the flexible Si–O–Si moiety.

The *trans*-silylation reaction with $O_2Si_3Cl_8$ yielded the asymmetrically substituted siloxane **7**, which has two pentacoordinate silicon atoms. Analysis of its ^{29}Si NMR shifts (CP/MAS measurements and quantum chemical calculations of the principal components of the CSA tensor) allowed for unequivocal assignment of the chemical shifts to the individual Si atoms of this compound. Dynamic behavior of the *Si*-bound pz* moieties was observed depending on the choice of the solvent, and coalescence was almost reached in $CDCl_3$.

Isolation of the fully substituted trisiloxane $O_2Si_3pz^*_8$ (**8**) by an optimized protocol showed the importance of the choice of the solvent. The comparison of the solution and solid-state ^{29}Si NMR spectra of **8** showed four-coordinated silicon atoms in both cases.

Experimental Section

General: All manipulations were performed under an inert atmosphere of dry argon by using standard Schlenk techniques or a MBraun Glovebox with a concentration of O_2 and H_2O below 5 ppm. $CDCl_3$ was distilled from CaH_2, *n*-hexane was distilled from sodium, *n*-pentane was dried with a column of molecular sieves, and C_6D_6 was used as received. All solvents were stored with molecular sieves under argon. Me_3SiCl, $O(SiMe_2Cl)_2$, $O(SiCl_3)_2$, $O(SiMePh_2)_2$, $AlCl_3$ (anhydrous), acetyl chloride, $O_2Si_3Cl_8$, and 3,5-dimethylpyrazole were used as received from commercial suppliers. Trimethyl-3,5-dimethylpyrazolylsilane (Me_3Sipz^*) was synthesized as described before.[1] Raman spectra were recorded with a Bruker Optik RFS 100/S spectrometer equipped with an Nd-YAG laser (1500 mW, 1064 nm) in the range 3600–90 cm^{-1}. Elemental analyses were carried out with a Vario Micro Cube analyzer of the company Elementar (Hanau, Germany).

1,1,3,3-Tetrachloro-1,3-dimethyldisiloxane [$O(SiMeCl_2)_2$, 1]: Acetyl chloride (19.1 g, 243.5 mmol) was added to a stirred suspension of anhydrous $AlCl_3$ (32.5 g, 234.5 mmol) and $O(SiMePh_2)_2$ (25.0 g, 60.9 mmol) in *n*-hexane (300 mL) at room temperature in several portions through a dropping funnel. The reaction commenced after a short induction period and proceeded in boiling *n*-hexane with occurrence of two liquid phases. After cooling the reaction mixture, the *n*-hexane phase was separated by decantation. Distillation at ambient pressure (details in Supporting Information) gave **1** as a colorless liquid (at 143 °C), yield 7.8 g, 32 mmol, 53 %. ^{1}H NMR (400.13 MHz, C_6D_6, 20 °C, TMS): δ = 0.47 ppm (s, 6 H, $SiCH_3$); ^{13}C{^{1}H} NMR (100.63 MHz, C_6D_6, 20 °C, TMS): δ = 5.4 ppm [^1J(Si,C) = 47.0 Hz, $SiCH_3$]; ^{29}Si{^{1}H} NMR (79.48 MHz, C_6D_6, 20 °C, TMS): δ = –15.0 ppm [$OSiCH_3(Cl_2)$]. Raman: $\tilde{\nu}$ = 142 (w), 173 (vw), 195 (vw), 232 (vw), 340 (vw), 446 (s) [Si–Cl], 1270 (vw), 1404 (vw), 2914 (vs), 2985 (w) cm^{-1}.

1,3-Bis(3,5-dimethylpyrazolyl)-1,1,3,3-tetramethyldisiloxane [$O(SiMe_2pz^*)_2$, 2]: Me_3Sipz^* (19.9 g, 118.4 mmol) was added to a stirred solution of $O(SiMe_2Cl)_2$ (12.0 g, 59.2 mmol) in *n*-hexane (50 mL), and the reaction mixture was heated to reflux for 9.5 h. After removal of the solvent and volatile components under reduced pressure (condensation into a cold trap), the raw product

was distilled in vacuo to yield **2** as a colorless liquid (126 °C, 2 mbar), yield 8.59 g, 26.6 mmol, 45 %. ^{1}H NMR (400.13 MHz, C_6D_6, 20 °C, TMS): δ = 5.71 (s, 2 H, pz*C-H), 2.11 (s, 12 H, pz*C-CH_3) 0.39 ppm [s, 12 H, Si(CH_3)$_2$]; ^{13}C{^{1}H} NMR (100.63 MHz, C_6D_6, 20 °C, TMS): δ = 151.13 (pz*C-CH$_3$), 145.6 (pz*C-CH$_3$), 107.9 (pz*C-H) 13.6 (pz*C-CH$_3$), 12.5 (pz*C-CH$_3$), 0.7 ppm [^1J(Si,C) = 36.0 Hz, Si(CH_3)$_2$]; ^{29}Si{^{1}H} NMR (79.48 MHz, C_6D_6, 20 °C, TMS): δ = –6.1 ppm [OSi(CH_3)$_2$pz*]. Raman: $\tilde{\nu}$ = 100 (vw), 171 (vw), 193 (vw), 412 (vw), 469 (vw), 491 (vw), 589 (w), 709 (vw), 799 (vw), 1019 (vw), 1443 (w), 1556 (vw), 2728 (vw), 2743 (vw), 2869 (w), 2905 (vs), 2922 (s), 2983 (m), 3090 (vw), 3123 (vw) cm^{-1}. $C_{14}H_{26}N_4OSi_2$ (322.56): calcd. C 52.13, H 8.12, N 17.73; found C 52.42, H 8.08, N 17.34.

1,1,3,3-Tetrakis(3,5-dimethylpyrazolyl)-1,3-dimethyldisiloxane [O(SiMepz*$_2$), 3]: Me$_3$Sipz* (2.2 g, 13.3 mmol) was added to a solution of O(SiMeCl$_2$)$_2$ (0.81 g, 3.3 mmol) in *n*-hexane (10 mL) and the mixture stirred at room temperature for 27 h. After evaporation of the solvent and volatile components, **3** was obtained as a colorless solid, yield 1.57 g, 3.25 mmol, 98 %, m.p. 95 °C (decomposition, sealed capillary). ^{1}H NMR (400.13 MHz, C_6D_6, 20 °C, TMS): δ = 5.68 (s, 4 H, pz*C-*H*), 2.05 (s, 24 H, pz*C-CH$_3$), 1.22 ppm (s, 6 H, SiCH$_3$); ^{13}C{^{1}H} NMR (100.63 MHz, C_6D_6, 20 °C, TMS): δ = 149.3 (pz*C-CH$_3$), 108.4 (pz*C-H), 12.7 (pz*C-CH$_3$), –0.6 ppm (SiCH$_3$); ^{29}Si{^{1}H} NMR (79.48 MHz, C_6D_6, 20 °C, TMS): δ = –36.3 ppm [OSiCH$_3$(pz*$_2$)]. Raman: $\tilde{\nu}$ = 84 (w), 117 (w), 167 (w), 188 (w), 209 (w), 343 (vw), 462 (vw), 593 (m), 1019 (w), 1441 (w), 1465 (w),1562 (vw), 2684 (vw), 2914 (vs), 2955 (w), 2976 (w) cm^{-1}. $C_{22}H_{34}N_8OSi_2$ (482.74): calcd. C 54.74, H 7.10, N 23.21; found C 54.65, H 7.20, N 22.97.

Hexakis(3,5-dimethylpyrazolyl)disiloxane [O(Sipz*$_3$)$_2$, 4]: Me$_3$Sipz* (9.14 g, 54.3 mmol) was added to a solution of O(SiCl$_3$)$_2$ (2.58 g, 9.0 mmol) in *n*-hexane (15 mL) and the mixture heated to reflux for 2.5 h. After cooling, a colorless solid formed, which was collected by filtration, washed with *n*-hexane (4 × 10 mL), and dried in vacuo, yield 5.16 g, 8.0 mmol, 88 %, m.p.114 °C (decomposition, sealed capillary). ^{1}H NMR (400.13 MHz, CDCl$_3$, 20 °C, TMS): δ = 5.82 (s, 6 H, pz*C-*H*), 2.02 ppm (s, 36 H, pz*C-CH_3); ^{13}C{^{1}H} NMR (100.63 MHz, CDCl$_3$, 20 °C, TMS): δ = 153.3 (pz*C-CH$_3$), 148.9 (pz*C-CH$_3$), 108.8 (pz*C-H), 13.2 (pz*C-CH$_3$) 12.2 ppm (pz*C-CH$_3$); ^{29}Si{^{1}H} NMR (79.48 MHz, CDCl$_3$, 20 °C, TMS): δ = –78.1 ppm (OSipz*$_3$). Raman: cm^{-1} $\tilde{\nu}$ = 111 (s), 201 (w), 288 (vw), 325 (vw), 363 (vw), 437 (vw), 591 (s), 647 (vw), 759 (vw), 797 (vw), 971 (vw), 1021 (w), 1085 (vw), 1144 (vw), 1310 (vw), 1372 (vw), 1439 (m), 1472 (w), 1567 (vw), 2730 (vw), 2867 (vw), 2922 (vs), 2964 (m), 3108 (vw) cm^{-1}. $C_{30}H_{42}N_{12}OSi_2$ (642.91): calcd. C 56.05, H 6.58, N 26.14; found C 56.25, H 6.66, N 26.15.

1,1-Dichloro-1,3,3,5,5,5-hexakis(3,5-dimethypyrazolyl)trisiloxane ([(pz*$_2$Si)(μ-pz*)O(Sipz*)(μ-pz*)O(SiCl$_2$pz*)], 7): Me$_3$Sipz* (2.70 g, 16.0 mmol) was added in one portion to a solution of $O_2Si_3Cl_8$ (0.80 g, 2.0 mmol) in *n*-hexane . The reaction mixture was stirred thoroughly for a few seconds and then stored undisturbed. After 48 h the crystallization of the product had finished. The supernatant solution was decanted, and the crystals washed with *n*-hexane (2 × 10 mL) and dried in vacuo. Compound **7** was obtained as a colorless solid, yield 1.13 g, 1.5 mmol, 74 %, m.p. 177 °C (decomposition, sealed capillary). Due to exchange reactions it is not possible to assign individual chemical shifts to the pyrazolyl units, so ranges for the components are reported. ^{1}H NMR (400.13 MHz, C_6D_6, 20 °C, TMS): δ = 5.78–5.43(6 H, pz*C-*H*), 2.49–1.86 ppm (36 H, pz*C-CH_3); ^{13}C{^{1}H} NMR (100.63 MHz, C_6D_6, 20 °C, TMS): δ = 149.3–146.5 (pz*C-CH$_3$), 110.3–107.3 (pz*C-H), 13.9–12.1 ppm (pz*C-CH$_3$); ^{29}Si{^{1}H} NMR (79.48 MHz, C_6D_6, 20 °C, TMS): δ = –133.3/–135.7 (*I*= 2/1, OSipz*$_2$O), –120.9/–121.2 (*I*=1/2, OSiCl$_2$pz*), –68 ppm (pz*$_3$*Si*O); ^{29}Si CP/MAS NMR (79.51 MHz, 20 °C, TMS): δ = –135.2 (OSipz*$_2$O), –123.8 (OSiCl$_2$pz*), –63.4 ppm (pz*$_3$SiO). Raman: $\tilde{\nu}$ = 100 (s), 149 (m), 202 (m), 241 (w), 267 (w), 307 (w), 328 (w), 367 (w), 462 (w), 497 (w), 535 (w), 593 (m), 968 (vw), 1020 (w), 1067 (vw), 1155 (vw), 1189 (vw), 1189 (vw), 1350 (vw), 1380 (vw), 1439 (m), 1467 (w), 1538 (vw),1556 (vw), 1574 (vw), 2732 (vw), 2866 (w), 2927 (vs), 2960 (m), 2982 (m), 2998 (w), 3109 (vw), 3129 (w) cm^{-1}. $C_{30}H_{42}Cl_2N_{12}O_2Si_3$ (757.91): calcd. C 47.54, H 5.59, N 22.18; found C 47.74, H 5.55, N 21.87.

Octakis(3,5-dimethylpyrazolyl)trisiloxane [O$_2$Si$_3$pz*$_8$, 8]: Me$_3$Sipz* (4.04 g, 24.0 mmol)was added to a solution of $O_2Si_3Cl_8$ (1.20 g, 3.0 mmol) in CH_2Cl_2 (8.0 mL), and the mixture heated to reflux for 6 h. After the solvent and volatile components were removed in vacuo, the residue was dissolved in *n*-pentane (8.0 mL) and stored in a refrigerator (8 °C). After 7 d a colorless precipitate appeared. The supernatant solution was removed by decantation and the solid immediately dried in vacuo. Compound **8** was obtained as a colorless solid, yield 1.52 g, 1.7 mmol, 58 %, m.p. 280 °C (decomposition, sealed capillary). ^{1}H NMR (500.13 MHz, C_6D_6, 20 °C, TMS): δ = 5.75 (8 H, pz*C-*H*), 2.30 (24 H, pz*C-CH_3); 1.90 ppm (24 H, pz*C-CH_3); ^{13}C{^{1}H} NMR (125.76 MHz, C_6D_6, 20 °C, TMS): δ = 155.2 (pz*C-CH$_3$), 143.9 (pz*C-CH$_3$), 108.7 (pz*C-H), 12.8 (pz*C-CH$_3$), 10.7 ppm (pz*C-CH$_3$); ^{29}Si{^{1}H} NMR (99.36 MHz, C_6D_6, 20 °C, TMS): δ = –77.0 (pz*$_3$SiO), –91.1 ppm (OSipz*$_2$O). Raman: $\tilde{\nu}$ = 101 (s), 149 (w), 203 (w), 269 (vw), 307 (w), 340 (vw), 462 (vw), 498 (vw), 535 (vw), 593 (s), 642 (vw), 699 (vw), 739 (vw), 776 (vw), 967 (vw), 1019 (vw), 1067 (vw), 1152 (vw), 1191 (vw), 1308 (vw), 1351 (vw), 1380 (vw), 1441 (w), 1537 (vw), 2733 (vw), 2928 (vs), 3128 (w) cm^{-1}. $C_{40}H_{56}N_{16}O_2Si_3$ (877.25): calcd. C 54.77, H 6.43, N 25.55; found C 54.53, H 6.21, N 25.39.

Single-Crystal Structure Determination: The XRD data sets were collected with a Stoe IPDS2 diffractometer by using Mo-K_α (λ = 0.71073 Å) radiation. The structures were solved by direct methods (SHELXS-97) and refined to convergence on F^2 against all of the independent reflections by the full-matrix, least-squares method with the SHELXL-97 program.[26] Non-hydrogen atoms were refined anisotropically, *C*-bound hydrogen atoms were refined in idealized positions (riding model), and *N*-bound H atoms were located as residual electron-density peaks and refined isotropically without restraints (Table 6).

CCDC 1470248 (for **4**), 1470251 (for **4·5**), 1470249 (for **6**), and 1470250 (for **7**) contain the supplementary crystallographic data for this paper. These data can be obtained free of charge from The Cambridge Crystallographic Data Centre.

NMR Spectroscopy: Solution NMR spectra were recorded with a Bruker DPX 400 spectrometer operating at 400.13 MHz (^{1}H) or Bruker Avance III 500 operating at 500.13 MHz (^{1}H). The spectra were referenced internally to TMS or residual (protic) solvent signals. The ^{29}Si solid-state CP/MAS NMR spectra were recorded with a Bruker Avance 400 MHz WB spectrometer operating at 79.51 MHz (^{29}Si) by using a 7 mm probe and a spinning frequency of 5 kHz, if not otherwise specified. The chemical shift scale was referenced to TMS.

Quantum Chemical Calculations: The DFT calculations were carried out by using Gaussian 03.[27] NMR shielding tensors were calculated with the Gauge-Independent Atomic Orbital method (GIAO)[28] by using the B3PW91[29] density functional in combination with the 6-311+G(2d,p)[30] basis set for all atoms, and the geometries from X-ray structure analyses. Calculated absolute shielding values were converted to relative shifts δ by means of the calculated shielding for tetramethylsilane at the same level of theory. Energy calculations and the relaxed PES scan (Gaussian 09)[31] were

Table 6. Selected crystallographic and refinement data for **4**, (**4**)(**5**)$_2$, **6**, and **7**.

	4	(**4**)(**5**)$_2$	**6**	**7**
Formula	$C_{30}H_{42}N_{12}OSi_2$	$C_{70}H_{102}Cl_8N_{28}O_3Si_6$	$C_{15}H_{22}Cl_4N_6OSi_2$	$C_{30}H_{42}Cl_2N_{12}O_2Si_3$
M [g mol^{-1}]	642.94	1835.94	500.37	757.93
T [K]	200(2)	150(2)	200(2)	180(2)
Crystal size [mm]	0.25 × 0.20 × 0.10	0.23 × 0.11 × 0.03	0.40 × 0.15 × 0.03	0.35 × 0.25 × 0.13
Crystal system	triclinic	monoclinic	monoclinic	triclinic
Space group	$P\bar{1}$	$C2/c$	$P2_1/m$	$P\bar{1}$
a [Å]	9.2409(8)	32.121(2)	12.0257(6)	8.0624(4)
b [Å]	9.9622(8)	9.0573(3)	7.1971(4)	14.0076(7)
c [Å]	10.9282(9)	30.554(2)	13.3270(7)	17.6607(8)
α [°]	68.525(7)	90	90	97.655(4)
β [°]	66.749(6)	99.681(5)	103.464(4)	100.215(4)
γ [°]	74.890(7)	90	90	100.352(4)
V [Å^3]/Z	852.20(12)/1	8762.4(9)/4	1121.75(10)/2	1902.67(16)/2
$\varrho_{calcd.}$ [g cm^{-3}]	1.253	1.392	1.481	1.323
μ(Mo-K_α) [mm^{-1}]	0.148	0.402	0.654	0.311
F(000)	342	3848	516	796
Θ range [°]	2.4 to 25.5	2.3 to 25.0	2.6 to 27.0	2.6 to 30.0
Measured reflections	10462	22496	15554	31503
Independent reflections	3153 (R_{int} = 0.0683)	7651 (R_{int} = 0.1000)	2637 (R_{int} = 0.0392)	11086 (R_{int} = 0.0323)
Completeness [%]	99.4	99.2	99.9	99.9
Data/restraints/parameters	3153/0/211	7651/0 /542	2637/0/172	11086/0/454
Goodness of fit on F^2	1.038	0.952	1.083	1.036
$R1$/$wR2$ [$I > 2\sigma(I)$]	0.0412/0.1060	0.0480/0.0846	0.0267/0.0700	0.0388/0.1010
$R1$/$wR2$ (all data)	0.0559/0.1132	0.1120/0.1021	0.0322/0.0738	0.0503/0.1074
Largest diff. peak/hole [e Å^3]	0.386/–0.232	0.374/–0.443	0.304/–0.274	0.457/–0.374

done with the B3PW91 density functional in combination with the 6-31G(d) basis set for all atoms, on the fully optimized geometries.

Supporting Information (see footnote on the first page of this article): 1. color figures of the presented crystal structures. 2. Details of the solid-state NMR measurements of **7**. 3. Relaxed PES scan of **4**, reaction enthalpies and atomic coordinates. 4. Details concerning the isolation of **1**.

Acknowledgments

The authors thank the German Research Foundation (DFG) and the TU Bergakademie Freiberg, Germany for financial support.

Keywords: Silicon · Siloxanes · Nitrogen heterocycles · Coordination modes · Density functional calculations

[1] a) M. A. Halcrow, *Dalton Trans.* **2009**, *38*, 2059–2073; b) S. Trofimenko, *Scorpionates. The coordination chemistry of polypyrazolborate ligands*, Imperial College Press, River Edge, NJ, **1999**; c) C. Pettinari, *Scorpionates II. Chelating Borate Ligands*, Imperial College Press, Covent Garden, **2008**; d) I. Kuzu, I. Krummenacher, J. Meyer, F. Armbruster, F. Breher, *Dalton Trans.* **2008**, 5836–5865; e) S. Styra, S. González-Gallardo, F. Armbruster, P. Oña-Burgos, E. Moos, M. Vanderach, P. Weis, O. Hampe, A. Grün, Y. Schmitt, M. Gerhards, F. Menges, M. Gaffga, G. Niedner-Schattenburg, F. Breher, *Chem. Eur. J.* **2013**, *19*, 8436–8446; f) F. Armbruster, T. Augenstein, P. Oña-Burgos, F. Breher, *Chem. Eur. J.* **2013**, *19*, 17899–17906.

[2] a) F. Bitto, J. Wagler, E. Kroke, *Eur. J. Inorg. Chem.* **2012**, 2402–2408; b) F. Bitto, K. Kraushaar, U. Böhme, E. Brendler, J. Wagler, E. Kroke, *Eur. J. Inorg. Chem.* **2013**, 2954–2962.

[3] a) K. A. Andrianov, A. I. Nogadielli, L. M. Khananashvili, D. S. Akhobadze, T. N. Vardosanidze, *Soobshch. Akad. Nauk Gruz. SSR* **1971**, *63*, 605–608; b) J. B. Davison, K. J. Wynne, *Macromolecules* **1978**, *11*, 186–191.

[4] N. Gotoh, T. Nakajima, j. H. Li, *Seisan Kenkyu* **1971**, *23*, 114–116.

[5] J. L. Webb, S. A. Nye, M. M. Grade, EP0398049A219901122, **1990**.

[6] Y. Inaki, *Polym. Mater. Sci. Eng.* **1989**, *60*, 165–169.

[7] a) A. N. Polivanov, N. N. Troitskaya, E. V. Los, N. N. Silkina, A. S. Shapatin, M. Gavars, O. D. Gracheva, A. G. Trufanov, V. N. Bochkarev, *Zh. Obshch. Khim.* **1987**, *57*, 1570–1573; b) M. Kumada, M. Yamaguchi, *Nippon Kagaku Zasshi* **1954**, *57*, 175–177.

[8] N. N. Sokolov, K. A. Andrianov, *Russ. Chem. Bull.* **1958**, *6*, 827–832.

[9] H. Manami, S. Nishizaki, *Nippon Kagaku Zasshi* **1958**, *79*, 60–65.

[10] a) A. G. Russell, T. Guveli, B. M. Kariuki, J. S. Snaith, *J. Organomet. Chem.* **2009**, *694*, 137–141; b) U. Herzog, H. Borrmann, *J. Organomet. Chem.* **2003**, *681*, 5–11; c) U. Herzog, H. Borrmann, *J. Organomet. Chem.* **2004**, *689*, 564–574.

[11] W. Wojnowski, W. Bochenska, K. Peters, E.-M. Peters, H. G. von Schnering, *Z. Anorg. Allg. Chem.* **1986**, *533*, 165–174.

[12] F. Weinhold, R. West, *Organometallics* **2011**, *30*, 5815–5824.

[13] G. Tsantes, N. Auner, T. Müller, in: *Organosilicon Chemistry V: From Molecules to Materials* (Eds.: J. Weis, N. Auner), Wiley-VCH, Weinheim, Germany, **2003**.

[14] G. V. Gibbs, M. B. Boisen, L. L. Beverly, K. M. Rosso, *Rev. Mineral. Geochem.* **2001**, *42*, 345–381.

[15] a) S. Vepachedu, R. T. Stibrany, S. Knapp, A. J. Potenza, H. J. Schugar, *Acta Crystallogr., Sect. C* **1995**, *51*, 423–426; b) F. Armbruster, I. Fernández, F. Breher, *Dalton Trans.* **2009**, 5612–5626.

[16] C. Glidewell, D. C. Liles, *J. Chem. Soc., Chem. Commun.* **1977**, 632–633.

[17] The structural factor τ is defined for five-coordinate geometries as $\tau = (\beta - \alpha)/60$ where α is the widest and β the second widest angle in the coordination sphere. $\tau = 1$ indicates an ideal trigonal bipyramid and $\tau = 0$ an ideal square pyramid as coordination polyhedron; see: A. W. Addison, T. N. Rao, J. Reedijk, J. van Rijn, G. C. Verschoor, *J. Chem. Soc., Dalton Trans.* **1984**, 1349–1355.

[18] a) N. Kocher, J. Henn, B. Gostevskii, D. Kost, I. Kalikhman, B. Engels, D. Stalke, *J. Am. Chem. Soc.* **2004**, *126*, 5563–5568; b) K. Akiba, in: *Chemistry of hypervalent compounds* (Ed.: K. Akiba), Wiley-VCH, New York, **1999**; c) C. Chuit, Robert J. P. Corriu, C. Reye, in: *Chemistry of hypervalent compounds* (Ed.: K. Akiba), Wiley-VCH, New York, **1999**.

[19] Determined according to the Herzfeld–Berger convention, see: J. Herzfeld, A. E. Berger, *J. Chem. Phys.* **1980**, *73*, 6021–6030.

[20] J. Mason, *Solid State Nucl. Magn. Reson.* **1993**, *2*, 285–288.

[21] R. K. Harris, E. D. Becker, S. M. C. De Menezes, P. Granger, R. E. Hoffman, K. W. Zilm, *Magnetic Resonance in Chemistry: MRC* **2008**, *46*, 582–598.

[22] E. Brendler, T. Heine, A. F. Hill, J. Wagler, *Z. Anorg. Allg. Chem.* **2009**, *635*, 1300–1305.

[23] L. E. Paul, I. C. Foehn, A. Schwarzer, E. Brendler, U. Böhme, *Inorg. Chim. Acta* **2014**, *423*, 268–280.

[24] a) L. A. Truflandier, E. Brendler, J. Wagler, J. Autschbach, *Angew. Chem. Int. Ed.* **2011**, *50*, 255–259; *Angew. Chem.* **2011**, *123*, 269–273; b) D. Gerlach, E. Brendler, T. Heine, J. Wagler, *Organometallics* **2007**, *26*, 234–240.

[25] a) D. H. O'Brien, C.-P. Hrung, *J. Organomet. Chem.* **1971**, *27*, 185–193; b) V. N. Torocheshnikov, N. M. Sergeyev, N. A. Viktorov, G. S. Goldin, V. G. Poddubny, A. N. Koltsova, *J. Organomet. Chem.* **1974**, *70*, 347–352.

[26] G. M. Sheldrick, *Acta Crystallogr., Sect. A* **2008**, *64*, 112–122.

[27] M. J. Frisch, G. W. Trucks, H. B. Schlegel, G. E. Scuseria, M. A. Robb, J. R. Cheeseman, J. A. Montgomery Jr., T. Vreven, K. N. Kudin, J. C. Burant, J. M. Millam, S. S. Iyengar, J. Tomasi, V. Barone, B. Mennucci, M. Cossi, G. Scalmani, N. Rega, G. A. Petersson, H. Nakatsuji, M. Hada, M. Ehara, K. Toyota, R. Fukuda, J. Hasegawa, M. Ishida, T. Nakajima, Y. Honda, O. Kitao, H. Nakai, M. Klene, X. Li, J. E. Knox, H. P. Hratchian, J. B. Cross, V. Bakken, C. Adamo, J. Jaramillo, R. Gomperts, R. E. Stratmann, O. Yazyev, A. J. Austin, R. Cammi, C. Pomelli, J. W. Ochterski, P. Y. Ayala, K. Morokuma, G. A. Voth, P. Salvador, J. J. Dannenberg, V. G. Zakrzewski, S. Dapprich, A. D. Daniels, M. C. Strain, O. Farkas, D. K. Malick, A. D. Rabuck, K. Raghavachari, J. B. Foresman, J. V. Ortiz, Q. Cui, A. G. Baboul, S. Clifford, J. Cioslowski, B. B. Stefanov, G. Liu, A. Liashenko, P. Piskorz, I. Komaromi, R. L. Martin, D. J. Fox, T. Keith, M. A. Al-Laham, C. Y. Peng, A. Nanayakkara, M. Challacombe, P. M. W. Gill, B. Johnson, W. Chen, M. W. Wong, C. Gonzalez, J. A. Pople, *Gaussian 03*, revision D.02, Gaussian, Inc., Wallingford CT, **2004**.

[28] K. Wolinski, J. F. Hinton, P. Pulay, *J. Am. Chem. Soc.* **1990**, *112*, 8251–8260.

[29] a) A. D. Becke, *J. Chem. Phys.* **1993**, *98*, 5648–5652; b) J. P. Perdew, Y. Wang, *Phys. Rev. B* **1992**, *45*, 13244–13249.

[30] a) W. J. Hehre, *Ab initio molecular orbital theory*, Wiley, New York, **1986**; b) P. C. Hariharan, J. A. Pople, *Theor. Chim. Acta* **1973**, *28*, 213–222; c) M. M. Francl, W. J. Pietro, W. J. Hehre, J. S. Binkley, M. S. Gordon, D. J. DeFrees, J. A. Pople, *J. Chem. Phys.* **1982**, *77*, 3654–3665.

[31] M. J. Frisch, G. W. Trucks, H. B. Schlegel, G. E. Scuseria, M. A. Robb, J. R. Cheeseman, G. Scalmani, V. Barone, B. Mennucci, G. A. Petersson, H. Nakatsuji, M. Caricato, X. Li, H. P. Hratchian, A. F. Izmaylov, J. Bloino, G. Zheng, J. L. Sonnenberg, M. Hada, M. Ehara, K. Toyota, R. Fukuda, J. Hasegawa, M. Ishida, T. Nakajima, Y. Honda, O. Kitao, H. Nakai, T. Vreven, J. A. Montgomery Jr., J. E. Peralta, F. Ogliaro, M. Bearpark, J. J. Heyd, E. Brothers, K. N. Kudin, V. N. Staroverov, R. Kobayashi, J. Normand, K. Raghavachari, A. Rendell, J. C. Burant, S. S. Iyengar, J. Tomasi, M. Cossi, N. Rega, J. M. Millam, M. Klene, J. E. Knox, J. B. Cross, V. Bakken, C. Adamo, J. Jaramillo, R. Gomperts, R. E. Stratmann, O. Yazyev, A. J. Austin, R. Cammi, C. Pomelli, J. W. Ochterski, R. L. Martin, K. Morokuma, V. G. Zakrzewski, G. A. Voth, P. Salvador, J. J. Dannenberg, S. Dapprich, A. D. Daniels, Ö. Farkas, J. B. Foresman, J. V. Ortiz, J. Cioslowski, D. J. Fox, *Gaussian 09*, revision D.01, Gaussian, Inc., Wallingford CT, **2013**.

Received: May 18, 2016
Published Online: August 16, 2016

